

The effects of network architecture on the photomechanical performance of azo-acrylate liquid crystal elastomers

Anastasiia Svanidze¹, Sudarshan Kundu¹, Olena Iadlovska¹,
Anil K.Thakur¹, Xiaoyu Zheng² and Peter Palffy-Muhoray^{1,2}

¹*Advanced Materials and Liquid Crystal Institute, Kent State University, OH, USA*

²*Department of Mathematical Sciences, Kent State University, OH, USA*

December 10, 2024

Abstract

Azo-containing liquid crystal elastomers are photomechanical materials which can be actuated by illumination. The photomechanical response is a result of the photoisomerization of the azo moiety, which produces bulk stresses in the material. These stresses arise via two distinct and competing mechanisms: order parameter change induced stress and direct contractile stress. We describe thermomechanical and photomechanical experiments aimed at assessing the relative contributions of these. we discuss our results and summarize our findings.

1 Introduction

Liquid crystal elastomers (LCEs) are a unique class of advanced materials that combine properties of liquid crystals and rubber-like materials. They consist of a crosslinked polymer network polymerized with monomers possessing liquid crystalline phases. LCEs, first proposed by P.G. de Gennes [1] and realized by H. Finkelmann [2], are remarkable materials [3] due to their exceptional responsiveness to external stimuli such as heating or illumination. This responsiveness originates from the sensitivity of liquid crystalline order to system parameters near a phase transition. LCEs hold significant potential for applications, as they can sustain and exert shear stresses as elastic solids. This makes them highly versatile for various applications requiring shape changes and stress response, such as soft robotics [4–6], artificial muscles [7, 8], adaptive optics [9], smart textiles [10–12] as well as biomedical applications [13–15]. The combination of mechanical flexibility and tunable properties makes LCEs well suited for next-generation responsive and adaptive technologies.

A great variety of LCEs has been synthesized, ranging from Finkelmann’s early polyhydrosiloxane-based ones [2, 16–21] to more recent acrylate-based [6, 22–32], polyester-based materials [33, 34] and others [35, 36]. Actuation mechanisms used to change the liquid crystal order parameter include heating [6, 7, 14, 22, 23, 25, 26], photoactuation [3, 4, 16–21, 24, 27, 29, 30, 37–43], the application of electric [44–46] and magnetic [47] fields and chemical stimuli [48].

In LCEs, photoactuation can be achieved by incorporating azobenzene moieties into the polymeric network. Upon illumination, the azobenzene undergoes photoisomerization, inducing internal stresses that can result in shape changes and enable the material to perform mechanical work. The photomechanical response can be attributed to two competing mechanisms: changes in the liquid crystal orientational order parameter, and direct contractile stress exerted on the network. In this work, we focus on amine-acrylate LCEs doped with azo dyes with different degrees of attachment to the network. We have measured and compared the thermal and photoresponse of three types of samples: those in which the azobenzene moiety is covalently bonded into the network at both ends (2-azo), at one end (1-azo) and not bonded at all (free-azo). In this paper, we describe our sample materials, report experimental results, discuss our findings in light of the two competing mechanisms and conclude by briefly summarizing our results.

2 Sample Composition and Structure

2.1 Materials

The chemical structure of the constituents of our samples are shown in Fig. 1. The liquid crystal monomer 1,4-Bis[4-(6-acryloyloxyhexyloxy)benzoyloxy]-2-methylbenzene (RM82) was purchased from Jiangsu Hecheng Advanced Materials Co., Ltd (China). The azo dyes 4,4'-Bis(6-acryloyloxyhexyloxy)azobenzene (2-azo) and acrylic acid (4-((4-hexyloxyphenyl) diazenyl)phenoxy)hexyl ester (1-azo) were purchased from SYNTHON Chemicals GmbH & Co. KG (Germany). The azo dye 1,2-Bis(4-(hexyloxy)phenyl)diazene (free-azo) was purchased, as result of custom synthesis, from Henan Daken Chemical Co., ltd (China). The chain extender N-butylamine and the photoinitiator phenylbis(2,4,6-trimethylbenzoyl)phosphine oxide (Irgacure 819) were purchased from Sigma-Aldrich, Merck KGaA (Germany). All materials were used as received; monomer purity was not taken into account in determining molar ratio. Polyimide SE-2170 (Nissan) and its thinner 21 (Nissan) for liquid crystal alignment were purchased from Brewer Science, Inc. (USA).

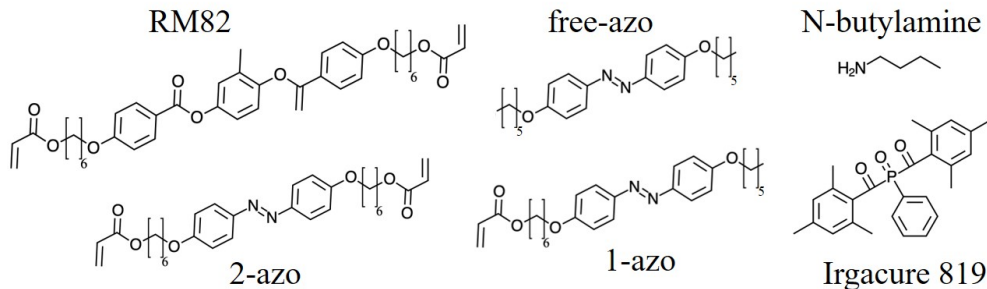


Figure 1: Chemical constituents of 2-azo, 1-azo and free-azo samples

Amine-acrylate-based LCEs were first proposed by T.J. White *et. al.* [23]; a number of the recipes are available for fabrication today [6, 22–27]. Below we briefly describe our fabrication process.

2.2 Network synthesis and sample production

Plain glass substrates, $10\text{ cm} \times 10\text{ cm} \times 1\text{ mm}$, were cleaned in ultrasonic bath with detergent at 60°C for 15 min followed by rinsing of substrates with DI water and IPA. Following this, substrates were dried in an oven for 15 min at 82°C . The polyimide mixture SE-2170, in proportion 1 : 3 with its thinner, was spin coated onto the clean substrates with the sequence: $1\text{ s} - 500\text{ rpm}$, $30\text{ s} - 1500\text{ rpm}$, $1\text{ s} - 50\text{ rpm}$. After spin coating, the polyimide was soft baked at 80°C on the hotplate for 5 min and then hard baked in the oven at 200°C for 45 min . The glass substrates were then cooled to room temperature, and were rubbed unidirectionally with velvet cloth on a rubbing block 10 – 15 times. They were subsequently cut into $4.5\text{ cm} \times 4.5\text{ cm}$ squares and assembled anti-parallel into cells using Mylar film (DuPont Teijin Films) as spacers and Norland Optical Adhesive 68T as glue.

The liquid crystal monomer, azo dye and photoinitiator were added to the amine and melted at 110°C while stirring for 30 s . The mass of the photoinitiator added was $2.5\text{ wt.}\%$ of the combined mass of the other constituents. Relative concentrations of the components of six samples are shown in Table 1.

Empty cells with planar surface alignment on the hotplate at 85°C were filled with the mixture via the capillary effect. Filled cells were moved to an oven at 77°C and left overnight for oligomerization.

The LCE cells were cured the following day using a mercury lamp (OmniCure s1500, Excelitas Technologies Corp. USA). A filter with cut-on wavelength 400 nm (20CGA-400, Newport, USA) was placed on each cell to reduce the photoisomerization of azobenzene during curing. Polymerization was carried out with light intensity of $75\text{ mW}/\text{cm}^2$ at 70°C for 20 min . Light intensity was measured at 405 nm with Optical Power Meter (1830-R, Newport, USA).

After curing, cells were heated to 100°C and opened using a thin blade. The LCE samples were removed from the substrate with tweezers.

Table 1: Compositions of sample types

sample type	RM82 (mole fraction)	azo dye (mole fraction)	acryl./amine (mole ratio)	Irgacure (wt. %)
no azo	1	0	1.1:1	2.5
free-azo 2%	0.98	0.02	1.1:1	2.5
1-azo 2%	0.98	0.02	1.1:1	2.5
2-azo 2%	0.98	0.02	1.1:1	2.5
free-azo 5%	0.95	0.05	1.1:1	2.5
1-azo 5%	0.95	0.05	1.1:1	2.5
2-azo 5%	0.95	0.05	1.1:1	2.5

The differences between samples are as follows: 2-azo samples contained azo molecules with two covalently bondable double bonds, 1-azo samples contained azo molecules with one covalently bondable double bond and free-azo samples contained azo molecules with no covalently bondable double bonds. All samples were produced using identical procedures, only the type (2-azo, 1-azo and free-azo) and percentage (2% or 5%) of azo compounds was changed.

A simple schematic of the resulting polymer network, shown in Fig. 2, illustrates the key structural differences.

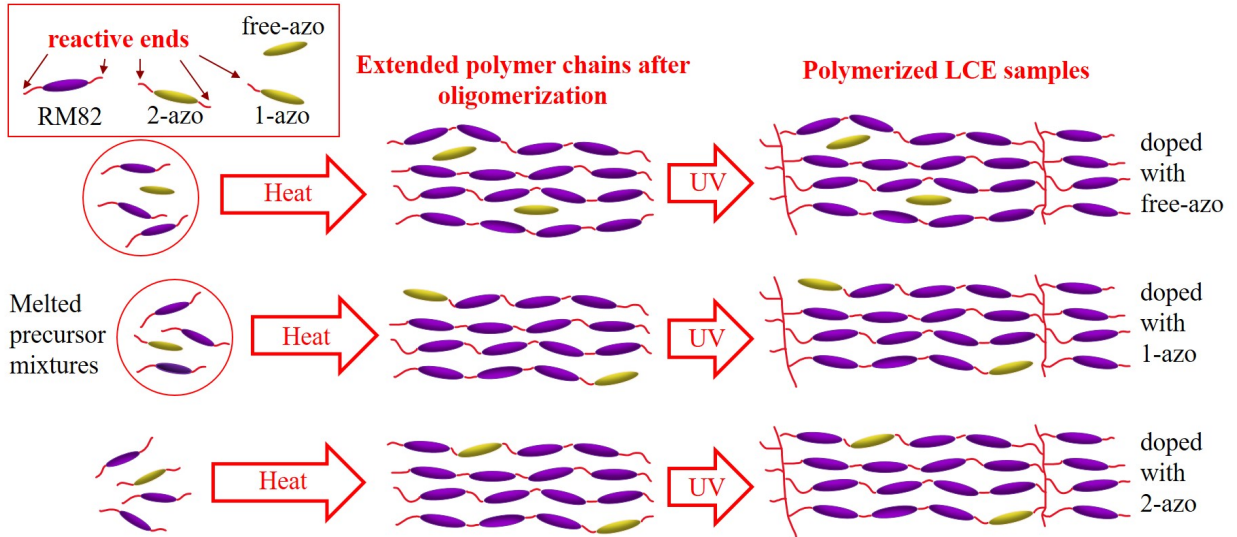


Figure 2: Networks of azo-doped acrylate based LCEs

3 Experimental Results

3.1 Elastic Moduli

Young's modulus of all samples was measured using custom-built apparatus [28]. For these measurements LCE samples were cut into $4\text{ mm} \times 20\text{ mm}$ strips with the director oriented parallel to the long edge. Samples marked with black dots were clamped at top and bottom and a tensile force was applied. A photograph of the sample was taken for each load and the strain was determined using ImageJ software [28]. A schematic of the device and experimental setup, together with typical data is shown in Fig. 3.

The LCE samples without any applied stress are not completely flat. Elongating a sample initially therefore requires very little stress, which then increases nonlinearly until the linear regime is reached. Measurements are shown in the linear regime. Data and Young's moduli for all samples are shown in Fig. 4.

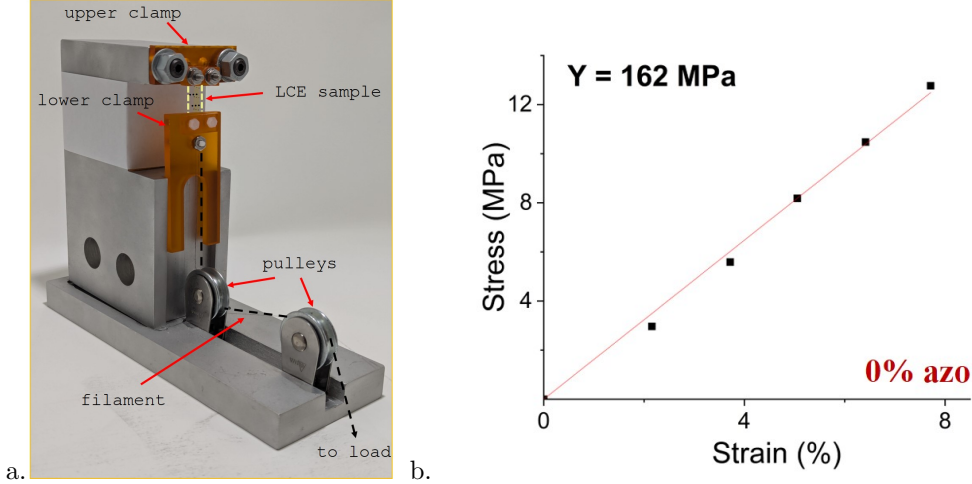


Figure 3: a. Tensile force apparatus. b. Young's modulus data for LCE sample with no azo dye.

3.2 Thermal Stress Measurements

Our samples for thermal and photostress measurements were 30 mm long, 10 mm wide and 27–32 μm thick, with nematic alignment along their long edge. They were held with the long edge vertical and their two 10 mm edges clamped between two rigid horizontal plexiglass struts leaving a 10 mm \times 10 mm sample area between holders. The bottom edge was held in fixed position by a rigid support, while the top was connected to an Entran force sensor, whose height could be adjusted, with a nearly inextensible thin (Fireline jewelry thread) filament. The sample and its holders were under water in a thermostatted container. An image of the setup, used for both thermal and photostress measurements, is shown in Fig. 5.

Thermal stress was determined by the following procedure. The initial stress on the sample was set by adjusting the height of the Entran sensor. The water temperature was increased in steps. At each temperature, the Entran voltage was recorded continuously for 1 min, and was then averaged over time to provide the force and then the stress exerted by the sample. The thermal stress was obtained by subtracting the initial stress from the measured stress. The heating rate between measurements was 0.25°C/min.

Thermal stress data from azo-containing samples is presented below together with photostress.

3.3 Transmission spectra

Photoactuation in these samples is due to photoisomerization of the azo moiety. When azo isomers, predominantly in the extended *trans*- configuration, absorb light at 365 nm, they undergo photoisomerization to the more compact *cis*- form, which has absorption peak near 450 nm. Information about dynamics of the population distribution can be inferred from transmission spectra.

We have illuminated our samples with light from a 500 mW LED at 365 nm. The intensity of the illumination was 250 mW/cm² with duration 10 s. We then measured the transmittance spectra, whose minima give information about the relative density of the *trans*- and *cis*- isomers, as function of time. Transmission measurements were performed using an HR4000CG-UV-NIR (Ocean Optics Inc., USA) spectrometer. Spectra were normalized with respect to the sample with no azo dye. The transmittance relaxation data is shown in Fig. 6.

Material and optical parameters of the samples are given in Table 2. The absorption cross-section is $\sigma = 1/(\rho l_d)$, where ρ is the number density, and l_d is the decay length.

Although transmittance is clearly higher for the 2% than for the 5% azo containing samples, there is very little difference in the extent of isomerization in the free-azo, 1-azo and 2-azo samples. We note here that the isomerization process is only weakly dependent on temperature, given the large excitation energy needed for azo *trans-cis* isomerization [29].

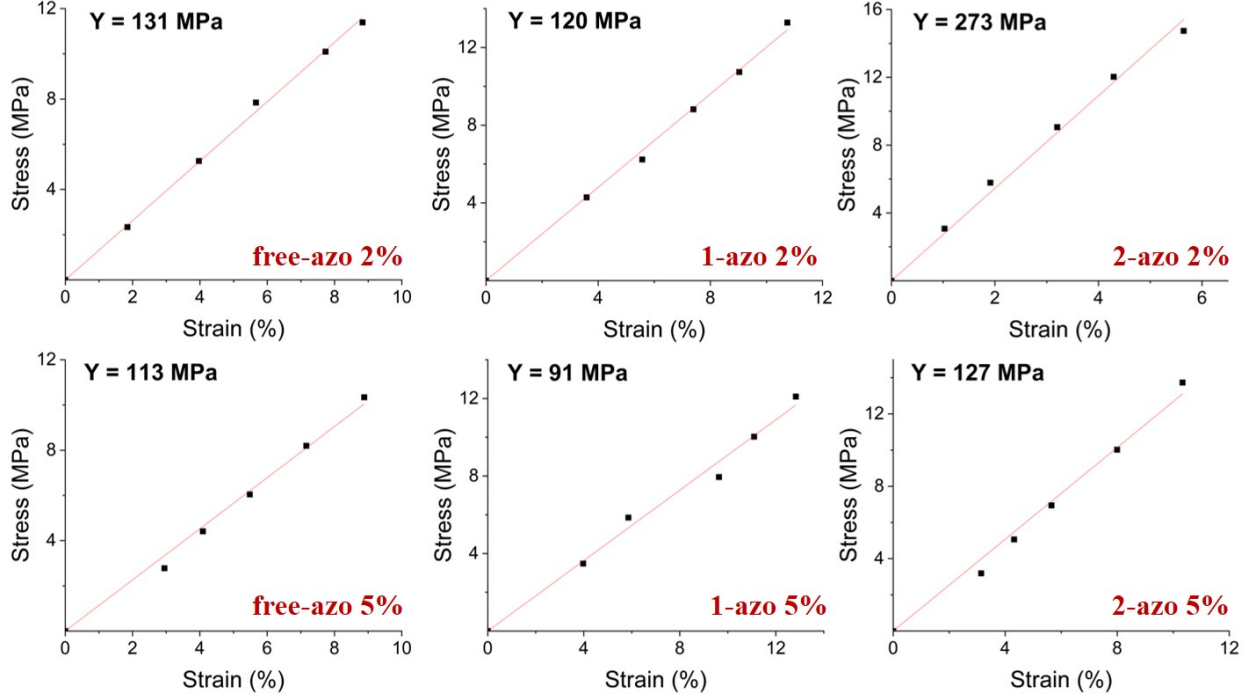


Figure 4: Young’s moduli data for all samples. Top and bottom rows are for 2% and 5% free-azo, 1-azo and 2-azo samples, respectively.

Table 2: Sample material and optical parameters

Sample	Thickness (μm)	Max Absorbance (Arb. units)	Number density of dye (m^{-3})	Decay length (μm)	Absorption cross-section (m^2)	Cis-lifetime (s)
free-azo 2%	27	0.43	1.86×10^{25}	63	8.5×10^{-22}	1.2×10^4
1-azo 2%	27	0.57	1.94×10^{25}	47	1.1×10^{-21}	9.3×10^3
2-azo 2%	28	0.82	1.97×10^{25}	34	1.49×10^{-21}	4.4×10^3
free-azo 5%	31	1.36	4.7×10^{25}	23	9.2×10^{-22}	5.9×10^3
1-azo 5%	32	1.61	4.64×10^{25}	20	1.08×10^{-21}	6.5×10^3
2-azo 5%	27	1.87	4.84×10^{25}	14	1.48×10^{-21}	3.6×10^3

3.4 Photostress and Thermal Stress Measurements

Photostress measurements were carried out using the same setup as thermal stress measurements, shown in Fig. 5. The sample was illuminated with UV light at 365 nm from a 500 mW LED (Prizmatix Ltd.) at a distance of 6 cm from the sample. The light source was unpolarized, so polarization dependent effects [30,42] need not be considered. The illuminated area of the sample was 10 mm \times 10 mm. The illumination sequence consisted of: UV OFF for 10 s, then, repeatedly, UV ON for 200 ms, UV OFF for 1 s. Since the *cis*-thermal relaxation time is very slow, as indicated in Table 2, after each measurement the sample was illuminated with light at 460 nm for 1 s to drive the *cis-trans* isomerization.

To illustrate that the photomechanical effect is result of the presence of azo dyes, we show the thermal and photoresponse of samples without azo dye in Fig. 7. There is no observable photostress in our thermostatted samples without azo dyes.

Photostress measurement results, together with those from thermal stress measurements, are shown in Figs. 8 and 9. The results of measurements clearly indicate that the thermal stresses are essentially identical for free-azo, 1-azo and 2-azo samples with the same initial stresses, however, photostresses of 2-azo samples differ dramatically from those of free-azo and 1-azo samples with the same initial stresses for both 2% and

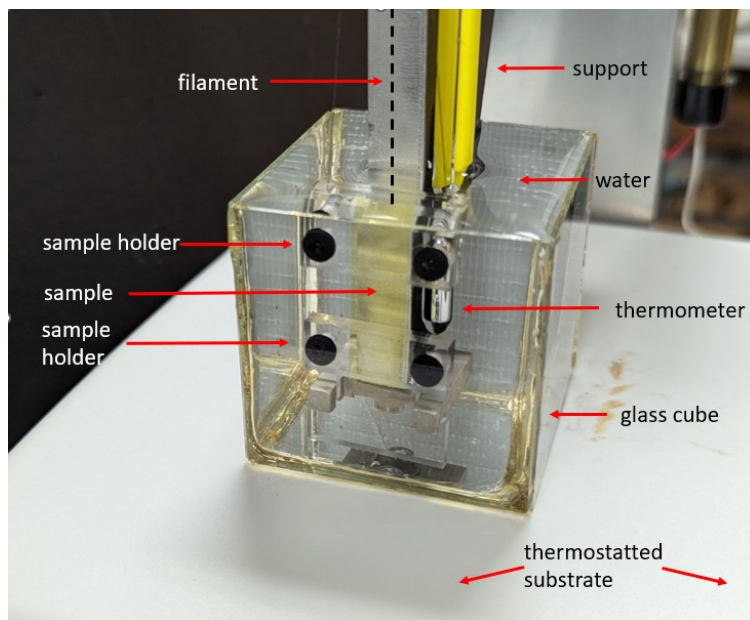


Figure 5: Thermal and photostress setup. The filament location is indicated by dashed line. Thermal insulation has been removed for visibility.

5% azo concentrations. Our interpretations of these results are elucidated in the following discussion section.

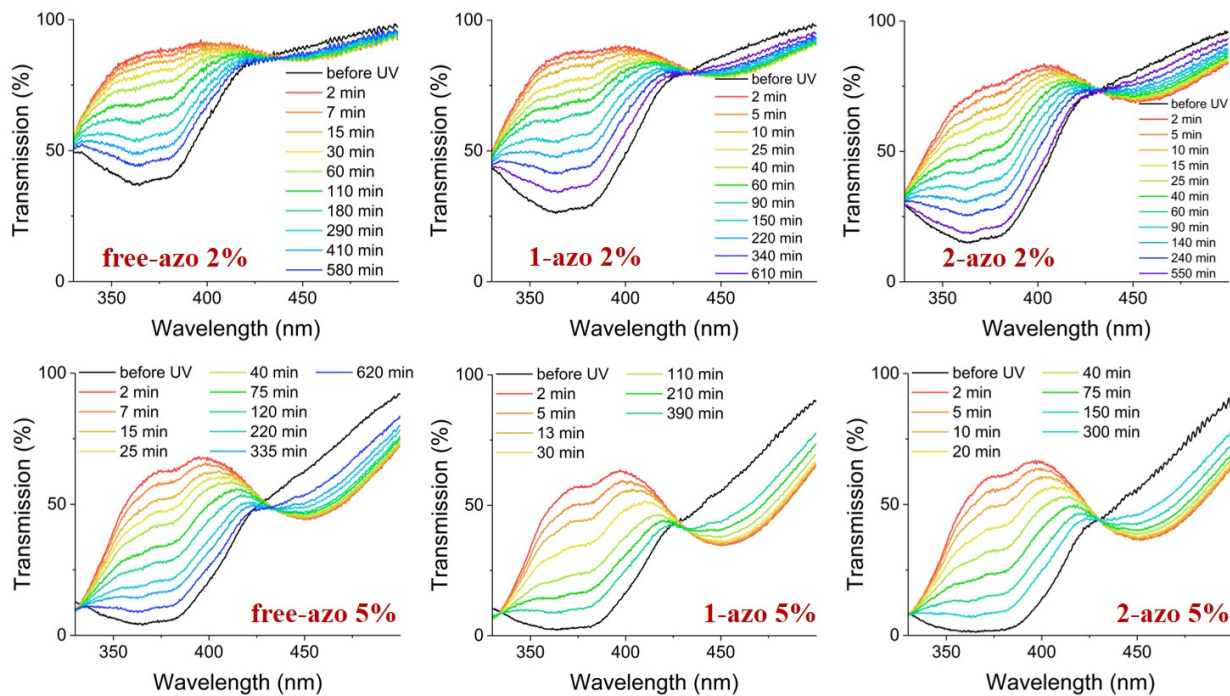


Figure 6: Transmission spectra of all samples. Top and bottom rows are for 2% and 5% of free-azo, 1-azo and 2-azo samples, respectively.

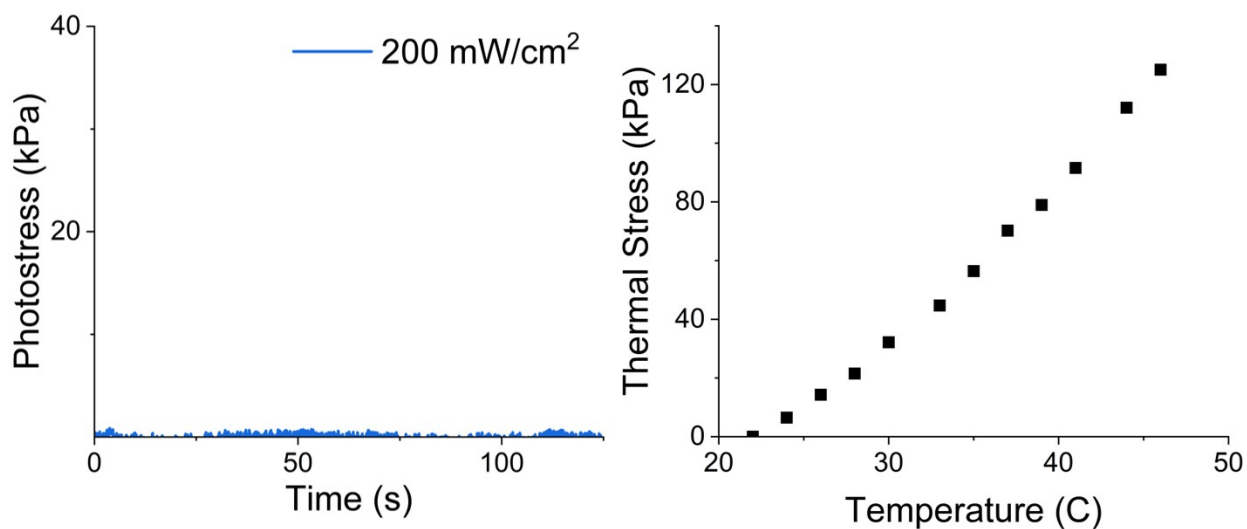


Figure 7: Photostress and thermal stress in acrylate LCE samples not containing azo dye. The initial stress is 50 kPa.

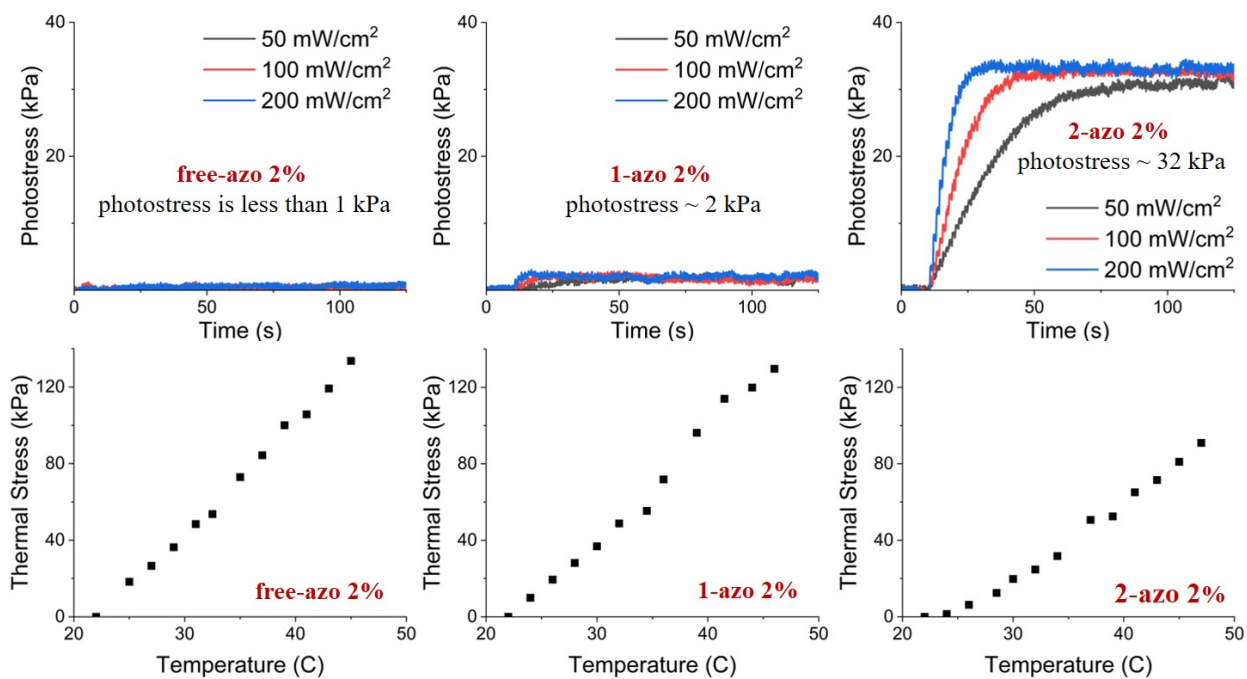


Figure 8: Photostress (top) and thermal stress (bottom) in acrylate LCE samples containing 2% 0-azo, 1-azo, and 2-azo dye. The initial stress is 50 kPa.

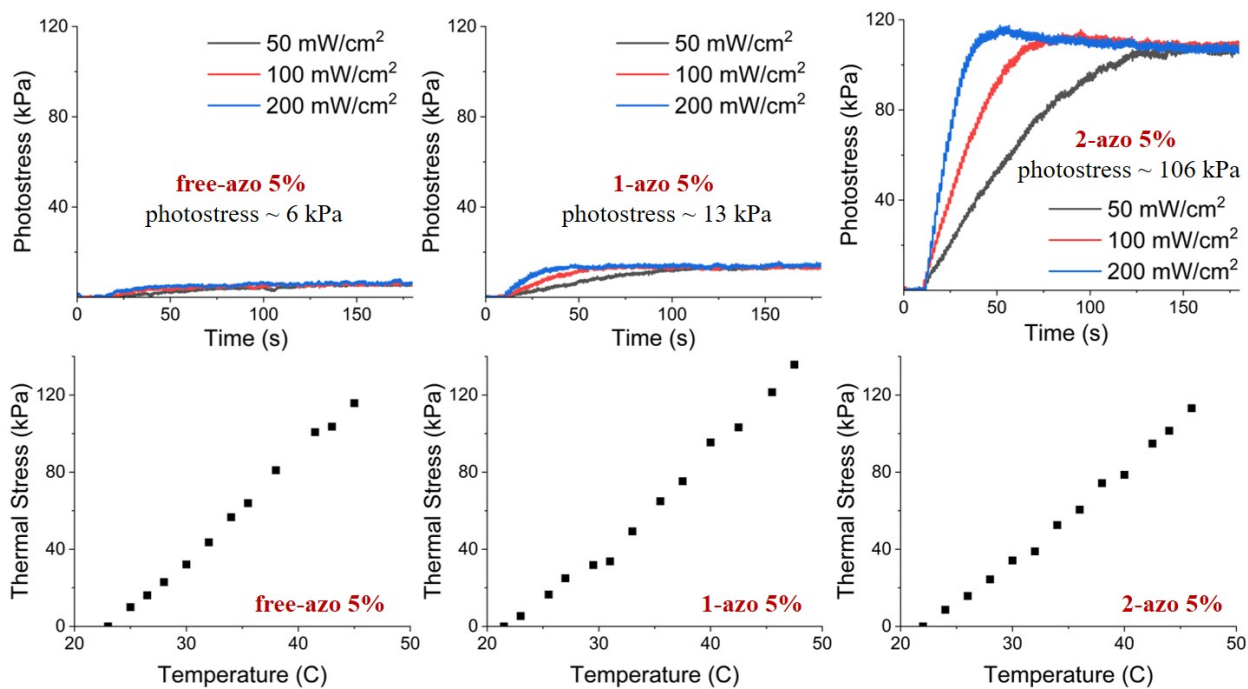


Figure 9: Photostress (top) and thermal stress (bottom) in acrylate LCE samples containing 5% 0-azo, 1-azo, and 2-azo dye. The initial stress is 90 kPa.

4 Discussion

Heating changes the orientational order of nematic liquid crystals, which is necessarily coupled to mechanical strain [1], [37]. This coupling persists in solid LC elastomers [3] and even in LC glasses [38]. Photoisomerization changes the shape of the azo-containing molecules. This gives rise to two competing mechanisms: 1. change in orientational order due to the azo-containing molecules being less liquid-crystal like (the shape is less elongated and the polarizability is less anisotropic), and 2. a direct contractile stress due to the contraction of the two ends of the aligned azo-mesogens due to photoisomerization.

The first of these, the change in orientational order parameter has often been referred to as the major mechanism for photoactuation in LCEs [16, 30, 37, 39, 41–43] and has been seen as playing essentially the same role in both thermal and photoactuation [40, 41, 43]. The second, direct contractile stress, was already recognized by Finkelmann and Sanchez [19] who referred to the mechanism as ‘cooperative effect’. Earlier studies have probed the effects of different azo dye attachments [17, 18], but the different structures of the dyes used made comparisons difficult. Later work on siloxane elastomers [19] with two different kinds of 2-azo and 1-azo dyes (also different from ours) indicated that higher photostress was exhibited by 2-azo samples. Although the justification is not clearly given in their paper, it is suggested that mechanism 2 provides 60% and mechanism 1 40% of the stress.

Our three samples, with the 2-azo, 1-azo and free-azo architectures, exhibit essentially identical thermal stress as shown in the bottom rows of Figs. 8 and 9. This implies that the differences in network architecture do not affect the thermally induced change in order parameter or the stress resulting from the order parameter change. The thermal stress is due to the change of order parameter caused by a change of temperature, and the stress is primarily the consequence of the coupling of the order parameter and the stress.

The three samples, with the 2-azo, 1-azo and free-azo architectures exhibit the same photoisomerization, as indicated by spectroscopic results shown in Fig. 6. If the photostress was primarily due to the change in order parameter via mechanism 1, then the photostress would be essentially the same for all samples, since the photoisomerization is essentially the same. If the photostress was primarily due to a direct contractile stress due to mechanism 2, then the result for the 2-azo sample would be dramatically different from the response of the 1-azo and free-azo samples. Since the difference in the observed photostress is dramatically larger for the 2-azo samples than those for the 1-azo and free-azo samples, we conclude that the primary mechanism is the contractile stress due to photoisomerization in mechanism 2.

In light of the above, it is interesting to ask: what then is the role of liquid crystallinity in the photoresponse of 2-azo samples? Likely the role is to provide alignment of the azo moiety when the sample is prepared. Acrylate LCEs, with or without azo compounds, are essentially aligned nematic samples, which would also align the predominantly *trans*- azo isomers. Our samples produce uniaxial stress because the stress-producing azo moiety is aligned, and the contraction of the unidirectionally aligned azo-nematogens, with their covalent bonds at two ends, efficiently transfer stress to the bulk network. It appears then that the main role of liquid crystallinity in the 2-azo samples is to provide the alignment of the stress-producing azo moieties for the production of unidirectional stress.

5 Summary

Our experimental results indicate that photostress created in 2-azo acrylate LCEs is due to direct unidirectional contraction of the network caused by shape change of the azo moiety during photoisomerization. Stress associated with order parameter change also exists, as observed in 1-azo and free-azo samples, but it is about one order of magnitude smaller than photostress in 2-azo materials. In the 2-azo samples, the traditional actuating mechanism via order parameter change is therefore not significant; the primary role of liquid crystallinity is simply to align the photoresponsive azo containing molecules during network formation.

6 Acknowledgements

We are grateful to Professors Dirk Broer and Danqing Liu for numerous enlightening discussions as well as some sample materials. We are indebted to Dr. Bahman Taheri of AlphaMicron Inc. who kindly presented

this work at ILCC2024 on our behalf. We acknowledge support in part from the Office of Naval Research through the MURI on Photomechanical Material Systems (ONR N00014-18-1-2624).

References

- [1] de Gennes, P.-G. Réflexions Sur Un Type de Polymères Nématiques. *CR Acad. Sci. Ser. B* **1975**, *281*, 101–103.
- [2] Finkelmann, H.; Kock, Hans-J.; Rehage, G. Investigations on Liquid-Crystalline Polysiloxanes .3. Liquid-Crystalline Elastomers - a New Type of Liquid-Crystalline Material. *Macromol. Rapid Commun.* **1981**, *2* (4), 317–322. <https://doi.org/10.1002/marc.1981.030020413>.
- [3] Warner, M.; Terentjev, E. M. Nematic Elastomers—a New State of Matter? *Prog. Polym. Sci.* **1996**, *21* (5), 853–891. [https://doi.org/10.1016/s0079-6700\(96\)00013-5](https://doi.org/10.1016/s0079-6700(96)00013-5).
- [4] Ahn, C.; Liang, X.; Cai, S. Bioinspired Design of Light-Powered Crawling, Squeezing, and Jumping Untethered Soft Robot. *Adv. Mater. Technol.* **2019**, *4* (7), 1900185. <https://doi.org/10.1002/admt.201900185>.
- [5] Wang, Z.; Guo, Y.; Cai, S.; Yang, J. Three-Dimensional Printing of Liquid Crystal Elastomers and Their Applications. *ACS Appl. Polym. Mater.* **2022**, *4* (5), 3153–3168. <https://doi.org/10.1021/acsapm.1c01598>.
- [6] López-Valdeolivas, M.; Liu, D.; Broer, D. J.; Sánchez-Somolinos, C. 4D Printed Actuators with Soft-Robotic Functions. *Macromol. Rapid Commun.* **2017**, *39* (5), 1700710. <https://doi.org/10.1002/marc.201700710>.
- [7] Ma, J.; Wang, Y.; Sun, J.; Yang, Z. Liquid Crystal Elastomer Hollow Fibers as Artificial Muscles with Large and Rapid Actuation Enabled by Thermal-Pneumatic Enhanced Effect. *Adv. Funct. Mater.* **2024**, *34* (37), 2402403. <https://doi.org/10.1002/adfm.202402403>.
- [8] Li, M.-H.; Keller, P. Artificial Muscles Based on Liquid Crystal Elastomers. *Phil. Trans. R. Soc. A* **2006**, *364* (1847), 2763–2777. <https://doi.org/10.1098/rsta.2006.1853>.
- [9] Ma, J.; Yang, Z. Chiral Liquid Crystal Elastomers Advance Light Modulation. *Light Sci. Appl.* **2024**, *13* (1), 205. <https://doi.org/10.1038/s41377-024-01549-4>.
- [10] Kim, S.-U.; Lee, Y.-J.; Liu, J.; Kim, D. S.; Wang, H.; Yang, S. Broadband and Pixelated Camouflage in Inflating Chiral Nematic Liquid Crystalline Elastomers. *Nat. Mater.* **2021**, *21* (1), 41–46. <https://doi.org/10.1038/s41563-021-01075-3>.
- [11] Roach, D. J.; Yuan, C.; Kuang, X.; Li, V. C. F.; Blake, P.; Romero, M. L.; Hammel, I.; Yu, K.; Qi, H. J. Long liquid crystal elastomer fibers with large reversible actuation strains for smart textiles and artificial muscles. *ACS Appl. Mater. Interfaces* **2019**, *11*(21), 19514–19521. <https://doi.org/10.1021/acsami.9b04401>.
- [12] Silva, P. E. S.; Lin, X.; Vaara, M.; Mohan, M.; Vapaavuori, J.; Terentjev, E. M. Active Textile Fabrics from Weaving Liquid Crystalline Elastomer Filaments. *Adv. Mater.* **2023**, *31*, 2210689. <https://doi.org/10.1002/adma.202210689>.
- [13] Prévôt, M.; Ustunel, S.; Hegmann, E. Liquid Crystal Elastomers—a Path to Biocompatible and Biodegradable 3D-LCE Scaffolds for Tissue Regeneration. *Materials* **2018**, *11* (3), 377. <https://doi.org/10.3390/ma11030377>.
- [14] Wu, J.; Yao, S.; Zhang, H.; Man, W.; Bai, Z.; Zhang, F.; Wang, X.; Fang, D.; Zhang, Y. Liquid Crystal Elastomer Metamaterials with Giant Biaxial Thermal Shrinkage for Enhancing Skin Regeneration. *Adv. Mater.* **2021**, *33* (45), e2106175. <https://doi.org/10.1002/adma.202106175>.

- [15] Hussain, M.; Jull, E. I.; Mandle, R. J.; Raistrick, T.; Hine, P. J.; & Gleeson, H. F. Liquid crystal elastomers for biological applications. *Nanomaterials* **2021**, *11*(3), 813. <https://doi.org/10.3390/nano11030813>.
- [16] Cviklinski, J.; Tajbakhsh, A.R.; Terentjev, E.M. UV Isomerisation in Nematic Elastomers as a Route to Photo-Mechanical Transducer. *Eur. Phys. J. E* **2002**, *9* (S1), 427–434. <https://doi.org/10.1140/epje/i2002-10095-y>.
- [17] Hogan, P. M.; Tajbakhsh, A. R.; Terentjev, E. M. UV Manipulation of Order and Macroscopic Shape in Nematic Elastomers. *Phys. Rev. E* **2002**, *65* (4), 041720. <https://doi.org/10.1103/physreve.65.041720>
- [18] Harvey, C. L. M.; Terentjev, E. M. Role of Polarization and Alignment in Photoactuation of Nematic Elastomers. *Eur. Phys. J. E* **2007**, *23* (2), 185–189. <https://doi.org/10.1140/epje/i2007-10170-y>
- [19] Sánchez-Ferrer, A.; Merekalov, A.; Finkelmann, H. Opto-Mechanical Effect in Photoactive Nematic Side-Chain Liquid-Crystalline Elastomers. *Macromol. Rapid Commun.* **2011**, *32* (8), 671–678. <https://doi.org/10.1002/marc.201100005>.
- [20] Dawson, N. J.; Kuzyk, M. G.; Neal, J.; Luchette, P.; Palffy-Muhoray, P. Modeling the Mechanisms of the Photomechanical Response of a Nematic Liquid Crystal Elastomer. *J. Opt. Soc. Am.* **2011**, *28* (9), 2134–2134. <https://doi.org/10.1364/josab.28.002134>.
- [21] Campos, J. G.; Tobin, C.; Sandlass, S.; Park, M.; Wu, Y.; Gordon, M.; Read, J. Photoactivation of Millimeters Thick Liquid Crystal Elastomers with Broadband Visible Light Using Donor-Acceptor Stenhouse Adducts. *Adv. Mater.* **2024**, *36*, 24044932. <https://doi.org/10.1002/adma.202404932>
- [22] Ware, T. H.; White, T. J. Programmed Liquid Crystal Elastomers with Tunable Actuation Strain. *Polym. Chem.* **2015**, *6* (26), 4835–4844. <https://doi.org/10.1039/c5py00640f>.
- [23] Ware, T. H.; McConney, M. E.; Wie, J. J.; Tondiglia, V. P.; White, T. J. Voxeled Liquid Crystal Elastomers. *Science* **2015**, *347* (6225), 982–984. <https://doi.org/10.1126/science.1261019>.
- [24] Ahn, S.; Ware, T. H.; Kyung Min Lee; Tondiglia, V. P.; White, T. J. Photoinduced Topographical Feature Development in Blueprinted Azobenzene-Functionalized Liquid Crystalline Elastomers. *Adv. Funct. Mater.* **2016**, *26* (32), 5819–5826. <https://doi.org/10.1002/adfm.201601090>.
- [25] Ambulo, C. P.; Burroughs, J. J.; Boothby, J. M.; Kim, H.; Shankar, M. R.; Ware, T. H. Four-Dimensional Printing of Liquid Crystal Elastomers. *ACS Appl. Mater. Interfaces* **2017**, *9* (42), 37332–37339. <https://doi.org/10.1021/acsami.7b11851>.
- [26] Kotikian, A.; Truby, R. L.; Boley, J. W.; White, T. J.; Lewis, J. A. 3D Printing of Liquid Crystal Elastomeric Actuators with Spatially Programed Nematic Order. *Adv. Mater.* **2018**, *30* (10), 1706164. <https://doi.org/10.1002/adma.201706164>.
- [27] Ceamanos, L.; Kahveci, Z.; López-Valdeolivas, M.; Liu, D.; Broer, D. J.; Sánchez-Somolinos, C. Four-Dimensional Printed Liquid Crystalline Elastomer Actuators with Fast Photoinduced Mechanical Response toward Light-Driven Robotic Functions. *ACS Appl. Mater. Interfaces* **2020**, *12* (39), 44195–44204. <https://doi.org/10.1021/acsami.0c13341>.
- [28] Oh, S.-W.; Guo, T.; Kuenstler, A. S.; Hayward, R.; Palffy-Muhoray, P.; Zheng, X. Measuring the Five Elastic Constants of a Nematic Liquid Crystal Elastomer. *Liq. Cryst.* **2020**, *48* (4), 511–520. <https://doi.org/10.1080/02678292.2020.1790680>.
- [29] Guo, T.; Svanidze, A.; Zheng, X.; Palffy-Muhoray, P. Regimes in the Response of Photomechanical Materials. *Appl. Sci.* **2022**, *12* (15), 7723. <https://doi.org/10.3390/app12157723>.
- [30] White, T. *Photomechanical Materials, Composites, and Systems : Wireless Transduction of Light into Work*; John Wiley & Sons, Ltd: Hoboken, NJ, USA, 2017.

- [31] Berrow, S. R.; Raistrick, T.; Mandle, R. J.; Gleeson, H. F. Structure–Property Relationships in Auxetic Liquid Crystal Elastomers—the Effect of Spacer Length. *Polymers* **2024**, *16* (14), 1957–1957. <https://doi.org/10.3390/polym16141957>.
- [32] Yakacki, C. M.; Saed, M.; Nair, D. P.; Gong, T.; Reed, S. M.; Bowman, C. N. Tailorable and Programmable Liquid-Crystalline Elastomers Using a Two-Stage Thiol–Acrylate Reaction. *RSC Adv.* **2015**, *5* (25), 18997–19001. <https://doi.org/10.1039/c5ra01039j>.
- [33] Yang, R.; Zhao, Y. Non-Uniform Optical Inscription of Actuation Domains in a Liquid Crystal Polymer of Uniaxial Orientation: An Approach to Complex and Programmable Shape Changes. *Angew. Chem. Int. Ed.* **2017**, *56* (45), 14202–14206. <https://doi.org/10.1002/anie.201709528>.
- [34] Beyer, P.; Braun, L.; Zentel, R. (Photo)Crosslinkable Smectic LC Main-Chain Polymers. *Macromol. Chem. Phys.* **2007**, *208* (22), 2439–2448. <https://doi.org/10.1002/macp.200700292>.
- [35] Lu, H.; Wang, M.; Chen, X.-M.; Lin, B.; Yang, H. Interpenetrating Liquid-Crystal Polyurethane/Polyacrylate Elastomer with Ultrastrong Mechanical Property. *J. Am. Chem. Soc.* **2019**, *141* (36), 14364–14369. <https://doi.org/10.1021/jacs.9b06757>.
- [36] Liu, X.-F.; Luo, X.; Liu, B.-W.; Zhong, H.-Y.; Guo, D.-M.; Yang, R.; Chen, L.; Wang, Y.-Z. Toughening Epoxy Resin Using a Liquid Crystalline Elastomer for Versatile Application. *ACS Appl. Polym. Mater.* **2019**, *1* (9), 2291–2301. <https://doi.org/10.1021/acsapm.9b00319>.
- [37] Warner, M.; Terentjev, E. M. *Liquid Crystal Elastomers, in international series of monographs on physics 120*; Clarendon Press: Oxford, UK, 2007.
- [38] Warner, M.; Modes, C. D.; Corbett, D.P. Curvature in Nematic Elastica Responding to Light and Heat. *Proc. R. Soc. A: Math.* **2010**, *466* (2122), 2975–2989. <https://doi.org/10.1098/rspa.2010.0135>.
- [39] Warner, M.; Terentjev, E. Thermal and Photo-Actuation in Nematic Elastomers. *Macromol. Symp.* **2003**, *200* (1), 81–92. <https://doi.org/10.1002/masy.200351008>.
- [40] Warner, M. Mechanical and Optical Bending of Nematic Elastomer Cantilevers. *Phys. Rev. E* **2012**, *86* (2), 022701. <https://doi.org/10.1103/physreve.86.022701>.
- [41] Warner, M.; Mahadevan, L. Photoinduced Deformations of Beams, Plates, and Films. *Phys. Rev. Lett.* **2004**, *92* (13), 134302. <https://doi.org/10.1103/physrevlett.92.134302>.
- [42] Corbett, D.; Warner, M. Nonlinear Photoresponse of Disordered Elastomers. *Phys. Rev. Lett.* **2006**, *96* (23). <https://doi.org/10.1103/physrevlett.96.237802>.
- [43] Corbett, D.; Warner, M. Changing Liquid Crystal Elastomer Ordering with Light – a Route to Opto-Mechanically Responsive Materials. *Liq. Cryst.* **2009**, *36* (10-11), 1263–1280. <https://doi.org/10.1080/02678290903062994>.
- [44] Fowler, H. E.; Rothmund, P.; Keplinger, C.; White, T. J. Liquid Crystal Elastomers with Enhanced Directional Actuation to Electric Fields. *Adv. Mater.* **2021**, *33* (43), 2103806. <https://doi.org/10.1002/adma.202103806>.
- [45] Urayama, K.; Honda, S.; Takigawa, T. Deformation Coupled to Director Rotation in Swollen Nematic Elastomers under Electric Fields. *Macromolecules* **2006**, *39* (5), 1943–1949. <https://doi.org/10.1021/ma052762q>.
- [46] Choi, M.-Y.; Kim, K.; Kim, K.; Ahn, S.; Na, J.-H. Rapid and Spatially Programmed Electrostatic Actuation of Anisotropic Polymers. *Chem. Eng. J.* **2023**, *475*, 146237. <https://doi.org/10.1016/j.cej.2023.146237>.
- [47] Winkler, M.; Kaiser, A.; Krause, S.; Heino Finkelmann; Schmidt, A. M. Liquid Crystal Elastomers with Magnetic Actuation. *Macromol. Symp.* **2010**, *291-292* (1), 186–192. <https://doi.org/10.1002/masy.201050522>.

- [48] Boothby, J. M.; Kim, H.; Ware, T. H. Shape Changes in Chemoresponsive Liquid Crystal Elastomers. *Sens. Actuators B: Chem.* **2017**, *240*, 511–518. <https://doi.org/10.1016/j.snb.2016.09.004>.